Improvement of Photovoltaic Performance of Colloidal Quantum Dot Solar Cells Using Organic Small Molecule as Hole-Selective Layer

Yaohong Zhang,[†,#] Guohua Wu,[‡,#] Iván Mora-Seró,[§] Chao Ding,[†] Feng Liu,[†] Qingxun Huang,[†] Yuhei Ogomi,[∥] Shuzi Hayase,[∥,⊥] Taro Toyoda,[†,⊥] Ruixiang Wang,[♯] Joe Otsuki,[,‡] Qing Shen[*,†,⊥]*

[†] Faculty of Informatics and Engineering, The University of Electro-Communications, 1-5-1 Chofugaoka, Chofu, Tokyo 182-8585, Japan.

[‡] College of Science and Technology, Nihon University, 1-8-14 Kanda Surugadai, Chiyoda-ku, Tokyo 101-8308, Japan.

[§] Institute of Advanced Materials (INAM), Universitat Jaume I, Av. de Vicent Sos Baynat, s/n 12006 Castelló de la Plana, Spain.

[∥] Faculty of Life Science and Systems Engineering, Kyushu Institute of Technology, 2-4 Hibikino, Wakamatsu-ku, Kitakyushu, Fukuoka 808-0196, Japan.

[⊥] CREST, Japan Science and Technology Agency (JST), 4-1-8 Honcho, Kawaguchi, Saitama 332-0012, Japan.

Beijing Engineering Research Centre of Sustainable Energy and Buildings, Beijing University of Civil Engineering and Architecture, No.15 Yongyuan Road, Huangcun, Daxing, Beijing 102616, China.

AUTHOR INFORMATION

Corresponding Author:

∗ Qing Shen. E-mail: shen@pc.uec.ac.jp; Fax: +81 42 443 5501; Tel: +81 42 443 5471.

∗ Joe Otsuki. E-mail: otsuki.joe@nihon-u.ac.jp; Fax: +81 3 3259 0817; Tel: +81 3 3259 0817.

Author Contributions

# These authors contributed equally to this work.

ABSTRACT

A novel organic small molecule bis-triphenylamine with spiro(fluorene-9,9'-xanthene) as the conjugated system, named BTPA-4, is successfully synthesized and employed as the hole-selective layer (HSL) in colloidal quantum dots solar cells (CQDSCs). The introduction of BTPA-4 layer can significantly prolong effective carrier lifetime (τ_{eff}), increase charge recombination resistance (R_{rec}), and thus diminish the interfacial charge recombination at the PbS-QDs/Au electrode interface. The effect of BTPA-4 as HSL in the device performance is especially significant for the open-circuit voltage (V_{oc}) and power conversion efficiency (*PCE*), with a ~ 10% and 15% enhancement respectively, comparing with those of device without the HSL. Furthermore, the PbS CQDSCs with BTPA-4 possessed a noticeably stable property for over 100 days of storage under ambient   atmosphere.

TOC Graphic
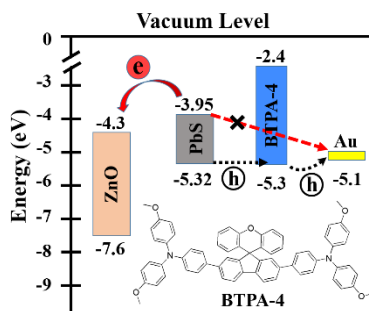
Colloidal quantum dots (CQDs) have been attracting immense attentions recently owing to their quantum-size effect bandgap tunability and low-cost solution processability.[1-2] This makes CQDs promising in various applications for instance field effect transistors (FETs),[3-5] light emitting diodes (LEDs),[6] and solar cells.[7-9] Colloidal quantum dots solar cells (CQDSCs), which are facile to fabricate by spin-coating procedure with low fabrication cost, have attracted worldwide interests as a promising candidate for the next generation solar cells. Recently, power conversion efficiency (*PCE*) of PbS CQDSCs has reached 12%.[10]

In order to effectively enhance the photovoltaic performance, various interfacial modifications in CQDSCs are vital issues.[8, 11] Considering the QDs layer in the first place, the surface defect states of QDs are the major constraints upon solar cell performance. Introducing the halide ligand, such as tetrabutylammonium iodide (TBAI) or PbI_2 to modify the surface of QDs is an effective way to enhance the coupling effect between QDs and reduce surface defect states of QDs.[12-19] Second, the use of appropriate charge selective contacts for both electrons and holes is a major issue in this kind of devices. For the photoanode/QDs interface, introducing an electron selecting layer between photoanode (ZnO or TiO_2, which have been the most commonly used) and the QDs active layer, and doping photoanode have been identified to significantly diminish the trap densities of photoanode and suppress the interfacial charge recombination at this interface.[20-26] For QDs/Au interface, the notion of inserting a hole-selective layer (HSL) between them has been proposed to suppress the interfacial charge recombination at this interface.[27-32] Molybdenum trioxide (MoO_3) has been introduced into PbS CQDSCs but those solar cells showed unstable properties due to the sensitivity of MoO_3 to H_2O and O_2.[27, 30, 33] An improved ZnO/PbS-TBAI/PbS-EDT (1,2-ethanedithiol) *n-i-p* architecture CQDSCs has promoted the *PCE* from 7.0% to 9.2%.[28] Unfortunately, the EDT ligand is easily desorbed from QDs surface when the device was exposed

to humid air in short time, reducing the stability and *PCE* of CQDSCs.[18, 34-35] Other hole transport materials such as poly(3-hexylthiophene-2,5-diyl) (P3HT) and 2,2',7,7'-tetrakis(*N,N*-di-*p*-methoxyphenylamine)-9,9'-spirobifluorene (Spiro-OMeTAD) have also been introduced into CQDSCs as a hole-selective/electron-blocking layer between QDs layer/Au electrode interface.[31, 36-38] However, high synthesis cost, complex purification, and the replicability especially for polymers are the major constraints upon their wide application. Great challenge should be taken to develop novel HSL with low cost and superior device stability.

Herein, we develop a novel donor-π-donor (D-π-D) organic small molecule bis-triphenylamine with spiro(fluorene-9,9'-xanthene) as the conjugated system, named BTPA-4, as a HSL in the PbS CQDSCs. We found that the introduction of BTPA-4 as HSL can enhance the open-circuit voltage (V_{oc}), prolong the effective carrier lifetime (τ_{eff}), reduce the recombination at PbS-QDs/Au interface, and hence improve the device performance. Furthermore, the PbS CQDSCs with BTPA-4 possessed a noticeably stable property for over 100 days of storage under ambient atmosphere that has been the Achilles' heel of other organic HSL for CQDSCs.
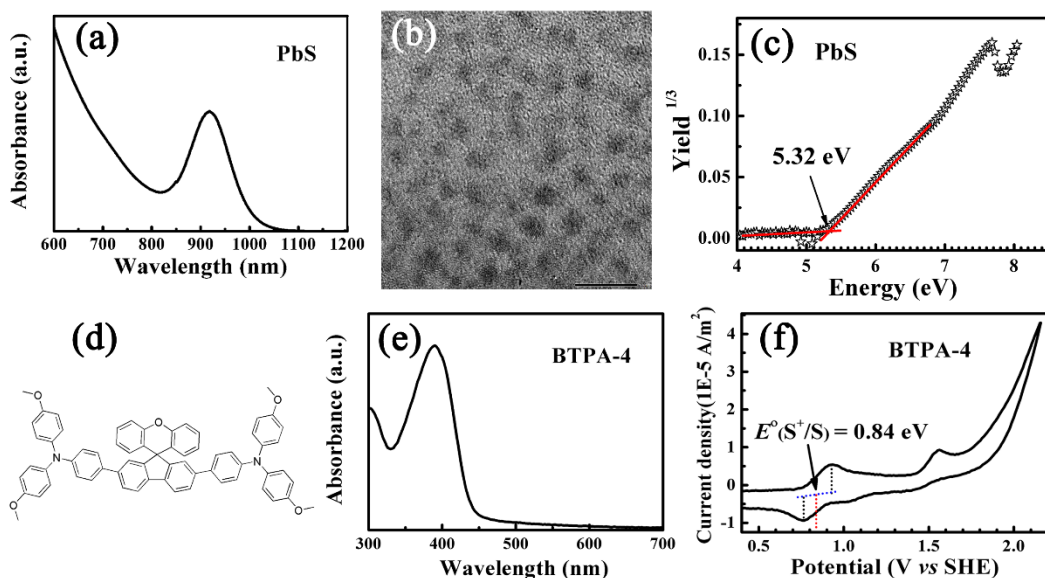
Figure 1. (a) Optical absorption spectrum of PbS-QDs in octane. (b) Transmission electron microscope (TEM) image of PbS-QDs, the scale bar represents 10 nm. (c) Photoelectron yield spectrum of PbS-QDs film which was treated with hexadecyltrimethylammonium bromide (CTAB). (d) Molecular structure of BTPA-4. (e) Optical absorption spectrum of BTPA-4 in dichloromethane (DCM). (f) Cyclic voltammogram in DCM, the potential values being obtained with ferrocene as the reference.

To clearly investigate the applicability of BTPA-4 in PbS CQDSCs, energy levels of PbS QDs and BTPA-4 were urgently needed. On one hand, PbS-QDs were synthesized by using a literature method.[25] Figure 1a shows the optical absorption spectrum of monodisperse PbS-QDs in octane. The first exciton absorption peak of PbS-QDs with the average size of PbS-QDs being approximately 2.7 nm in diameter, as shown in Figure 1b, is at 910 nm, which corresponds to its band gap energy of 1.36 eV. After solid state surface ligand exchange, the valence band maximum (VBM) position of the PbS-QDs film, which was treated by CTAB, was located at -5.32 eV as obtained by using photoelectron yield spectroscopy (Figure 1c). On the other hand, the molecular structure of BTPA-4 is depicted in Figure 1d (^{1}H NMR, ^{13}C NMR and HRMS spectra of BTPA-4 are shown in Figure S1, Figure S2 and Figure S3, respectively), and the band gap (2.9 eV) of BTPA-4 can be calculated from the intersection of its absorption spectrum, which is shown in Figure 1e, and normalized fluorescence spectrum (Figure S4). The highest occupied molecular orbital (HOMO) energy level of BTPA-4 was theoretically obtained from the following equation: $E_{HOMO} = -4.5 - E°(S^{+}/S)$ (eV), where $E°(S^{+}/S)$ is the first oxidation potential value vs SHE (standard hydrogen electrode),[39] which was obtained from cyclic voltammetry, Figure 1f, as 0.84 V. Thus, the HOMO energy level of BTPA-4 can be calculated approximately as -5.3 eV.
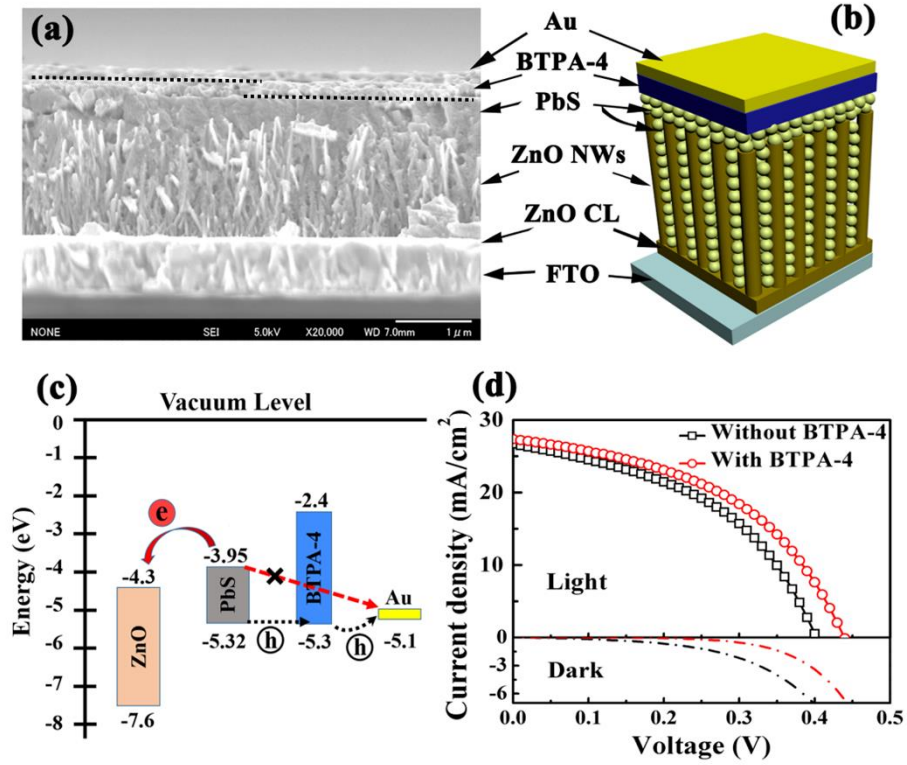
Figure 2. (a) Cross-section scanning electronic microscopy (SEM) image of the ZnO-NWs/PbS-QDs/BTPA-4/Au CQDSCs. (b) Schematic diagram of the *n-i-p* architecture PbS CQDSCs. (c) Schematic energy level diagram of the ZnO, PbS-QDs, BTPA-4, and Au. (d) The current density-voltage (*J-V*) curves of PbS CQDSCs with or without BTPA-4 as hole-selective layer.

The cross-section SEM image of PbS CQDSCs is shown in Figure 2a, which confirms the *n-i-p* structure of the device as illustrated in Figure 2b. It can be concluded that the thickness of the BTPA-4 layer is approximately 200 nm. Especially the BTPA-4 layer well contacts both with the PbS-QDs layer and the Au electrode. Figure 2c displays the energy level alignment in ZnO nanowires (NWs)/PbS-QDs/BTPA-4/Au solar cells, where the energy levels of PbS-QDs and BTPA-4 were calculated from the above discussion,[25, 40-41] while the energy level values of ZnO and Au were obtained from literature.[7, 25] It is shown that the HOMO level energy of BTPA-4 matches well with that of PbS QDs, which can provide an unimpeded access for the hole transport

7

from PbS-QDs layer to Au electrode. In contrast, the lowest unoccupied molecular orbital (LUMO) energy of the BTPA-4 is higher than that of PbS-QDs, which can set up an energy barrier for electron injection from PbS-QDs to Au electrode. It indicates that BTPA-4 has the potential as a hole-selective (or electron-blocking) layer to be used in the PbS CQDSCs.

Figure 2d shows J-V curves of PbS CQDSCs with and without BTPA-4 under the light and dark condition, and their corresponding performance parameters are shown in Table 1. The introduction of BTPA-4 layer strongly enhances the performance of PbS CQDSCs. The short-circuit photocurrent density (J_{sc}) of PbS CQDSCs shows no significant difference, see Figure S5. The addition of the HSL does not produce an increase of the series resistance (R_s) of the device as it has been analyzed by impedance spectroscopy (IS), see Figure S6. However, the best PbS CQDSCs with BTPA-4 HSL shows a PCE of 5.55%, which is around 15% higher than that without BTPA-4 layer (4.84%), mainly due to V_{oc} enhancement. Although the V_{oc} and J_{sc} of PbS CQDSCs with BTPA-4 HSL are slightly lower than those of PbS CQDSCs with PbS-EDT (see Figure S7 and Table S1), the fill factor (FF) of PbS CQDSCs with BTPA-4 is larger than that of device with PbS-EDT, resulting in a higher PCE. As a comparison to BTPA-4, a commonly used hole transport material Spiro-OMeTAD, with "spiro" structure in common with BTPA-4, also was introduced into PbS CQDSCs. Analogous to the devices with BTPA-4, the V_{oc} of PbS CQDSCs with Spiro-OMeTAD also were improved than that of the pristine devices (see Figure S8 and Table S2). However, comparing with PbS CQDSCs with BTPA-4, the V_{oc} for the devices based on Spiro-OMeTAD is lower. This can be explained by the fact that Spiro-OMeTAD (-5.2 eV) has a higher HOMO energy level than that of BTPA-4 (-5.3 eV).[42-43] BTPA-4 can also work as HSL for different sizes PbS-QDs based CQDSCs (see Figure S9 and Table S3), due to little changes in HOMO level of PbS-QDs with different sizes of PbS-QDs (E_g >1.2 eV).[35, 44]

These results confirm that the incorporation of the BTPA-4 layer between the PbS-QDs layer and Au electrode forming a *n-i-p* heterojunction structure, is feasibly successful. On one hand, this architecture avoids a Schottky barrier at the PbS-QDs layer/Au electrode interface,[32] resulting in devices with higher *FF*. On the other hand, BTPA-4 can block the electron injection from PbS-QDs to Au electrode, owing its high LUMO energy level (see Figure 2c).

Table 1. Performance details of PbS CQDSCs with and without BTPA-4 layer. Light intensity for the measurement is AM1.5 G 100 mW/cm^2 ^{a}

Devices	J_{sc} (mA/cm^2)	V_{oc} (V)	*FF* (%)	*PCE* (%)
Without BTPA-4	26.8±0.3 (26.6)	0.396±0.008 (0.402)	45.1±0.4 (45.3)	4.72±0.12 (4.84)
With BTPA-4	27.2±0.3 (27.0)	0.439±0.005 (0.442)	46.1±0.5 (46.5)	5.44±0.11 (5.55)

^{a} Statistics for each type solar cells are based on 8 devices. The values for champion devices are shown in the parentheses. All the devices were stored and measured in air.
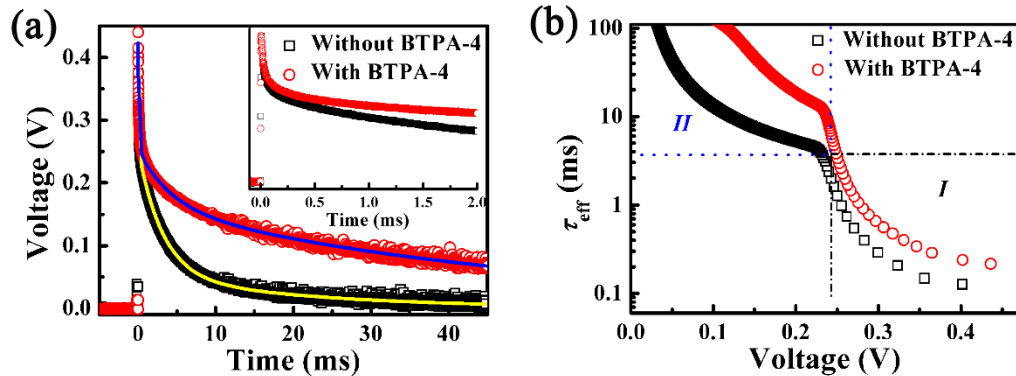
Figure 3. (a) Transient V_{oc} decay curves of PbS CQDSCs with and without BTPA-4. Inset is an expanded scale of the short time region of the decay showing the fast V_{oc} decay process of PbS CQDSCs. (b) Effective carrier lifetime (τ_{eff}) of PbS CQDSCs which were calculated from the V_{oc} decay curves shown in (a).

Transient V_{oc} decay measurements were used to reveal the effect of BTPA-4 as HSL on charge carrier recombination in PbS CQDSCs. Figure 3a shows the transient V_{oc} decay curves of PbS CQDSCs with and without the BTPA-4 layer. It can be clearly observed that samples with BTPA-4 exhibit a much slower decay, which provides a direct proof of the reduction of charge recombination when BTPA-4 is used as a HSL. Generally, in our samples, three photovoltage decay paths are observed: (1) hole trapping in PbS-QDs and electron trapping in ZnO-NWs,[25] (2) charge recombination at ZnO-NWs/PbS-QDs interface, and (3) charge recombination at PbS-QDs/Au electrode interface. Thus, the transient V_{oc} decay curves can be roughly split into three parts corresponding to these three charge recombination paths in the PbS CQDSCs. To clearly analyze the transient V_{oc} decay processes, the decay curves can be fitted by a triple exponential decay from the following equation:

$$y(t) = A_1 e^{-t/\tau_1} + A_2 e^{-t/\tau_2} + A_3 e^{-t/\tau_3} \quad (1)$$

where A_1, A_2 and A_3 are proportionality constants and τ_1, τ_2 and τ_3 are time constants.[45] The fitted curves are shown in Figure 3a (solid lines) and their corresponding parameters are shown in Table S4. According to the fitting data, for the fast voltage decay process, τ_1 and τ_2 are similar for samples with and without BTPA-4, which should belong to photovoltage decay path (1) and path (2), respectively. Interestingly, for the slow voltage decay process, τ_3 of PbS CQDSCs with BTPA-4 is increased from 21.2 ms to 50.8 ms. This relatively slower V_{oc} decay process of PbS CQDSCs with BTPA-4 may be caused by the suppressed interfacial recombination at PbS-QDs/Au electrode interface.

To further study the charge recombination processes, we investigated the τ_{eff} in PbS CQDSCs as well, which can be defined by the following equation:[45-47]

$$\tau_{eff} = -\left(\frac{kT}{q}\right)\bigg/\left(\frac{dV_{oc}}{dt}\right) \quad (2)$$

in which k represents the Boltzmann constant, T stands for the temperature, and q represents the elementary charge. Interestingly, the photovoltage-dependent τ_{eff} curves are clearly composed of two sections, I and II, see Figure 3b. In section I, the values of τ_{eff} for both PbS CQDSCs with and without BTPA-4 are close and below 3 ms. It indicates that the BTPA-4 layer has a reduced effect on this recombination process. In section II, the value of τ_{eff} in PbS CQDSCs with BTPA-4 is about 5 times higher than those without BTPA-4. This means that the slower recombination in section II is mostly caused by the PbS-QDs/Au interfacial recombination. Given these results, it can be concluded that BTPA-4 as HSL can significantly diminish the recombination between PbS-QDs and Au, therefore enhance the V_{oc} and PCE.
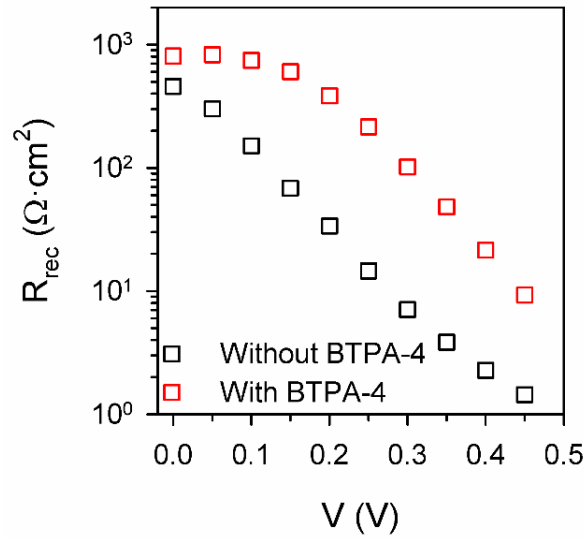
Figure 4. Recombination resistance (R_{rec}) of devices with and without BTPA-4 obtained by impedance spectroscopy.

Impedance spectroscopy provides a complementary characterization pointing also in this direction. Recombination resistance, R_{rec}, of both kinds of samples has been obtained by fitting the impedance spectra using equivalent circuits plotted in Figure S6, according to the reported work of Wang et al.[48] The sum of the low and intermediate frequency resistances, see Figure S6, are

directly related with the R_{rec} of the system, allowing a qualitative interpretation of the recombination process. Figure 4 shows the R_{rec} obtained for samples with and without BTPA-4. As R_{rec} is inversely proportional to the recombination rate, impedance measurements confirm the lower recombination in the devices with the HSL as demonstrated by the lower dark currents and the transient open circuit photovoltage decay measurements, in Figure 2d and Figure 3a, respectively.
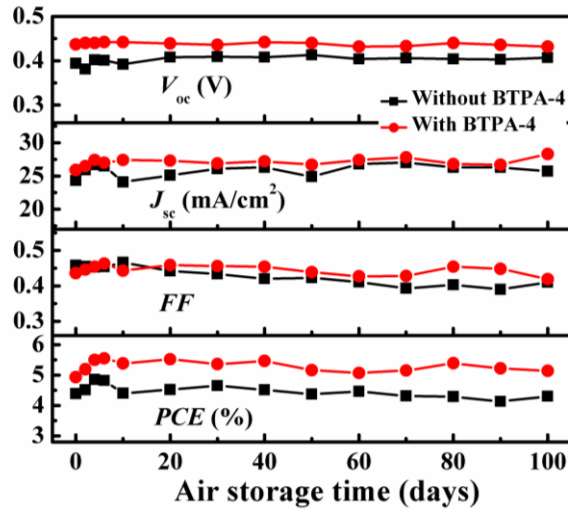
Figure 5. Stability evaluation of PbS CQDSCs with and without BTPA-4. The devices were stored and measured at room temperature (~ 20°C) with the indoor relative humidity of 28% ~ 65%.

The stability is a very important issue for the performance evaluation of CQDSCs. Therefore, we also investigated the long-term stability of PbS CQDSCs with and without BTPA-4 layer, which were kept and tested in air without the control of humidity. As shown in Figure 5, both the PbS CQDSCs with and without BTPA-4 exhibit excellent stable properties for over 100 days and the photovoltaic parameters exhibited overall increase at the first 8 days. After 100 days, the *PCE* of PbS CQDSCs with BTPA-4 can maintain 5.14% which is a little decrease compared with its maximum value. The *PCE* value of PbS CQDSCs with BTPA-4 is still higher than that of PbS

CQDSCs without BTPA-4 (4.3%), especially for V_{oc}. This result indicates that BTPA-4 is stable enough for the application as a HSL of CQDSCs.

In summary, organic small molecule BTPA-4 which has a suitable energy level was used into PbS CQDSCs as an effective hole-selective interlayer between the PbS-QDs and Au. By introducing the BTPA-4 layer, *PCE* of PbS CQDSCs was considerably improved. BTPA-4 as hole-selective layer can effectively inhibit the interfacial charge recombination between PbS-QDs and Au, and lead to the enhanced V_{oc}, which was explored by using transient V_{oc} decay and *IS* measurements in details. The BTPA-4 greatly reduced the interfacial charge recombination, increasing consequently the effective carrier lifetime in PbS CQDSCs. Due to the diminished interfacial recombination in the solar cells, the *PCE* of PbS CQDSCs with BTPA-4 is obtained as high as 5.55%, which shows a about 15% increase comparing with that without BTPA-4 and maintains it in the long-term period (over 100 days). This research demonstrates that BTPA-4 as a successful hole-selective material has the potential to be applied in other class photovoltaic devices such as perovskite solar cells.

EXPERIMENTAL METHODS

Synthesis of colloidal PbS-QDs. Colloidal PbS-QDs was synthesized by a similar method as shown in our previous literature.[25] Briefly, 6 mmol PbO was added into a mixed solution of OA (15 mmol) and 1-octadecene (ODE, 50 mL), which was degassed and stirred at 80°C for 1 h. Under nitrogen flow, the limpid solution was heated to 85°C and stirred for another 2 h with the subsequent injection of the hexamethyldisilathiane (TMS, 3 mmol) in pre-degassed ODE solution. When the obtained colloid solution was gradually cooling to 70°C, a $CdCl_2$-TDPA-oleylamine halide precursor was injected. After the mixture solution was completely cooling, PbS-QDs were

collected by adding acetone/methanol mixture solution and centrifugation process. The obtained PbS-QDs precipitate was dried by an N_2 flow and followed by dispersion in octane (50 mg/mL).

Synthesis of BTPA-4. A solution of *N,N*-bis(4-methoxyphenyl)-4-(4,4,5,5-tetramethyl-1,3,2-dioxaborolan-2-yl)benzenamine (354 mg, 0.82 mmol), spiro-9-(2,7-dibromofluorene)-9'-xanthene (200 mg, 0.41 mmol), K_2CO_3 (2 M solution, 0.5 mL), and a common catalyst $Pd(PPh_3)_4$ (40 mg, 0.04 mmol) in THF (15 mL) was heated to 95°C and continuously stirred for 48 h under nitrogen in the dark condition. The cooling mixture was subsequently extracted with about 100 mL $CHCl_3$. After dried by anhydrous $MgSO_4$, the $CHCl_3$ layer was obtained and concentrated by evaporator to give the residue. Finally, the residue was purified by chromatography eluted with hexane/ethyl acetate (5/1) to give a yellow solid BTPA-4 (weight: 210 mg, mole: 0.22 mmol, yield: 55%). ^{1}H NMR (400 MHz, CDCl$_3$): δ ppm: 7.82 (d, 2 H, J = 7.6 Hz), 7.59 (d, 2 H, J = 9.6 Hz), 7.37 (s, 2 H), 7.33 (d, 4 H, J = 8.8 Hz), 7.25 (t, 2 H, J = 6.8 Hz), 7.19 (t, 2 H, J = 7.6 Hz), 7.06 (m, 8 H), 6.93 (m, 4 H), 6.83 (d, 8 H, J = 9.2 Hz), 6.78 (d, 2 H, J = 8.0 Hz), 6.55 (d, 2 H, J = 7.6 Hz), 3.79 (s, 12 H). ^{13}C NMR (100 MHz, CDCl$_3$): δ ppm: 155.8, 155.7, 151.3, 148.0, 140.8, 140.7, 137.8, 132.7, 128.1, 128.0, 127.3, 126.4, 126.1, 125.0, 123.5, 123.3, 120.6, 120.0, 116.6, 114.6, 55.4, 54.3. APCI-HRMS *m/z* ([M+H]$^+$): calcd: 939.3798, Found: 939.4090. Anal. calcd for $C_{65}H_{50}N_2O_5 \cdot 0.2$ CHCl$_3$: C, 81.32; N, 2.91; H, 5.25. Found: C, 81.18; N, 2.93; H, 5.17.

Fabrication of solar cells. PbS-QDs-based bulk heterojunction CQDSCs were fabricated by combining the ZnO-NWs arrays with the PbS-QDs. The ZnO-NWs arrays with 1.5 μm thickness were formed on ZnO compact layer (ZnO-CL) by using a commonly used hydrothermal method. By using a layer-by-layer technique, PbS-QDs layers were deposited on ZnO-NWs arrays. Here, each layer was obtained by spin coating (2500 rpm,15 s). Firstly, colloidal PbS-QDs octane solution (50 mg/mL, 120 μL) was spin-cast onto the ZnO-NWs arrays. After that, CTAB methanol

solution (30 mM, 400 μL) was dropped on the substrate. One minute later, the substrate was spun dry and followed by rinsing three times with methanol. The PbS-EDT layers was covered on PbS-CTAB layer by EDT (0.02% vol., 400 μL) acetonitrile (CH_3CN) solution for 1 min before being spun. The formed spinning substrates were rinsed by 400 μL of CH_3CN and spun dry. The above process was repeated to obtain two layers of PbS-EDT. The BTPA-4 layer was spin coated (4000 rpm, 30 s) on the PbS-QDs layer by using the mixture of BTPA-4 (10 mM) in 0.5 mL chlorobenzene as well as 28.8 μL 4-*tert*-butylpyridine and 17.5 μL lithium bis (trifluoromethane)sulfonimide (520 mg/mL in CH_3CN) as the dopants. The Spiro-OMeTAD layer was covered on the PbS-QDs layer by spin-casting (4000 rpm, 30 s) the similar mixture solution as BTPA-4 but with 61 mM Spiro-OMeTAD and half dopants. At last, 100 nm Au electrode was deposited onto the HSL by thermal evaporation.

Characterization. The absorption spectra of colloidal PbS-QDs and BTPA-4 were obtained by using a UV−vis-NIR spectrophotometer (JASCO, V-670). The photoelectron yield spectrum was collected using a BIP-KV205 ionization energy measurement system (Bunkoukeiki). TEM (JEOL, JEM-2100F) and SEM (JEOL, JSM-6340) techniques were applied to measure the size of PbS-QDs and the morphology of solar cell, respectively. Cyclic voltammetry measurements of BTPA-4 (1 mM) were performed in CH_2CL_2 solution by adding 0.1 M tetrabutylammonium hexafluorophosphate ($TBAPF_6$) supporting electrolyte with a conventional three-electrode system which was composed of working (Pt disk), counter (Pt wire), and a pseudo-reference (Ag wire) electrodes. All the potentials were obtained by calibrating with reference to the internal ferricenium/ferrocene couple.[49] The *J-V* characteristics of PbS CQDSCs were performed under AM 1.5G irradiation (100 mW cm^{-2}) which was provided by a Peccell solar simulator (PEC-L10), and recorded by using a Keithley 2400 digital source meter. Incident photon to current conversion

efficiency (*IPCE*) spectra of PbS CQDSCs was measured by using a 300 W Xe arc lamp which was equipped with a Nikon G250 monochromator. The transient V_{oc} decay curves were obtained by using a pulsed YAG laser (wavelength 532 nm, repetition rate 4 Hz, pulse width 5 ns). The *IS* measurements were obtained by applying a bias from 0 to 0.45 V (amplitude 0.01 V) with a frequency ranging from $1E^6$ Hz to 1 Hz on a SP-300 (BioLogic) impedance analyzer.

ASSOCIATED CONTENT

Supporting Information. ^{1}H NMR, ^{13}C NMR, HRMS spectra, and fluorescence spectra, *IPCE* spectra, impedance spectroscopy and equivalent circuits, *J-V* curves and corresponding performance parameters of PbS CQDSCs with BTPA-4 and with PbS-EDT as hole-selective layer, *J-V* curves and corresponding performance parameters of PbS CQDSCs with BTPA-4 and with spiro-OMeTAD as hole-selective layer, *J-V* curves and corresponding performance parameters of different sizes PbS-QDs based CQDSCs with BTPA-4.

AUTHOR INFORMATION

Corresponding Author

* Qing Shen. E-mail: shen@pc.uec.ac.jp; Fax: +81 42 443 5501; Tel: +81 42 443 5471.

* Joe Otsuki. E-mail: otsuki.joe@nihon-u.ac.jp; Fax: +81 3 3259 0817; Tel: +81 3 3259 0817.

Author Contributions

# These authors contributed equally to this work.

Notes

REFERENCES

(1)   Kamat, P. V. Quantum Dot Solar Cells. The Next Big Thing in Photovoltaics. *J. Phys. Chem. Lett.* **2013,** *4*, 908-918.

(2)   Mora-Seró, I.; Bisquert, J. Breakthroughs in the Development of Semiconductor-Sensitized Solar Cells. *J. Phys. Chem. Lett.* **2010,** *1*, 3046-3052.

(3)   Osedach, T. P.; Zhao, N.; Andrew, T. L.; Brown, P. R.; Wanger, D. D.; Strasfeld, D. B.; Chang, L.-Y.; Bawendi, M. G.; Bulovic, V. Bias-Stress Effect in 1,2-Ethanedithiol-Treated PbS Quantum Dot Field-Effect Transistors. *ACS Nano* **2012,** *6*, 3121-3127.

(4)   Zhang, J.; Tolentino, J.; Smith, E. R.; Zhang, J.; Beard, M. C.; Nozik, A. J.; Law, M.; Johnson, J. C. Carrier Transport in PbS and PbSe QD Films Measured by Photoluminescence Quenching. *J. Phys. Chem. C* **2014,** *118*, 16228-16235.

(5)   Nugraha, M. I.; Loi, M. A.; Nugraha, M. I.; Hausermann, R.; Watanabe, S.; Takeya, J.; Watanabe, S.; Matsui, H.; Sytnyk, M.; Heiss, W.; et al. Broadening of Distribution of Trap States in PbS Quantum Dot Field-Effect Transistors with High-k Dielectrics. *ACS Appl. Mater. Interfaces* **2017,** *9*, 4719-4724.

(6)   Caruge, J. M.; Halpert, J. E.; Wood, V.; Bulovic, V.; Bawendi, M. G. Colloidal Quantum-Dot Light-Emitting Diodes with Metal-Oxide Charge Transport Layers. *Nat. Photon.* **2008,** *2*, 247-250.

(7)   Wang, H.; Kubo, T.; Nakazaki, J.; Kinoshita, T.; Segawa, H. PbS-Quantum-Dot-Based Heterojunction Solar Cells Utilizing ZnO Nanowires for High External Quantum Efficiency in the Near-Infrared Region. *J. Phys. Chem. Lett.* **2013,** *4*, 2455-2460.

(8)   Kim, M. R.; Ma, D. Quantum-Dot-Based Solar Cells: Recent Advances, Strategies, and Challenges. *J. Phys. Chem. Lett.* **2015,** *6*, 85-99.

(9)   Jiao, S.; Du, J.; Du, Z.; Long, D.; Jiang, W.; Pan, Z.; Li, Y.; Zhong, X. Nitrogen-Doped Mesoporous Carbons as Counter Electrodes in Quantum Dot Sensitized Solar Cells with a Conversion Efficiency Exceeding 12%. *J. Phys. Chem. Lett.* **2017,** *8*, 559-564.

(10)   NREL. *Efficiency Chart*; 2017.

(11)   Milliron, D. J. Quantum Dot Solar Cells: The Surface Plays a Core Role. *Nat. Mater.* **2014,** *13*, 772-773.

(12)   Tang, J.; Kemp, K. W.; Hoogland, S.; Jeong, K. S.; Liu, H.; Levina, L.; Furukawa, M.; Wang, X.; Debnath, R.; Cha, D.; et al. Colloidal-Quantum-Dot Photovoltaics Using Atomic-Ligand Passivation. *Nat. Mater.* **2011,** *10*, 765-771.

(13)   Brown, P. R.; Kim, D.; Lunt, R. R.; Zhao, N.; Bawendi, M. G.; Grossman, J. C.; Bulović, V. Energy Level Modification in Lead Sulfide Quantum Dot Thin Films through Ligand Exchange. *ACS Nano* **2014,** *8*, 5863-5872.

(14) Kim, S.; Noh, J.; Choi, H.; Ha, H.; Song, J. H.; Shim, H. C.; Jang, J.; Beard, M. C.; Jeong, S. One-Step Deposition of Photovoltaic Layers Using Iodide Terminated PbS Quantum Dots. *J. Phys. Chem. Lett.* **2014,** *5*, 4002-4007.

(15) Woo, J. Y.; Ko, J.-H.; Song, J. H.; Kim, K.; Choi, H.; Kim, Y.-H.; Lee, D. C.; Jeong, S. Ultrastable PbSe Nanocrystal Quantum Dots via in Situ Formation of Atomically Thin Halide Adlayers on PbSe(100). *J. Am. Chem. Soc.* **2014,** *136*, 8883-8886.

(16) Crisp, R. W.; Kroupa, D. M.; Marshall, A. R.; Miller, E. M.; Zhang, J.; Beard, M. C.; Luther, J. M. Metal Halide Solid-State Surface Treatment for High Efficiency PbS and PbSe QD Solar Cells. *Sci. Rep.* **2015,** *5*, 9945.

(17) Marshall, A. R.; Young, M. R.; Nozik, A. J.; Beard, M. C.; Luther, J. M. Exploration of Metal Chloride Uptake for Improved Performance Characteristics of PbSe Quantum Dot Solar Cells. *J. Phys. Chem. Lett.* **2015,** *6*, 2892-2899.

(18) Cao, Y.; Stavrinadis, A.; Lasanta, T.; So, D.; Konstantatos, G. The Role of Surface Passivation for Efficient and Photostable PbS Quantum Dot Solar Cells. *Nat. Energy* **2016,** *1*, 16035.

(19) King, L. A.; Parkinson, B. A. Photosensitization of ZnO Crystals with Iodide-Capped PbSe Quantum Dots. *J. Phys. Chem. Lett.* **2016,** *7*, 2844-2848.

(20) Liu, H.; Tang, J.; Kramer, I. J.; Debnath, R.; Koleilat, G. I.; Wang, X. H.; Fisher, A.; Li, R.; Brzozowski, L.; Levina, L.; et al. Electron Acceptor Materials Engineering in Colloidal Quantum Dot Solar Cells. *Adv. Mater.* **2011,** *23*, 3832-3837.

(21) Kim, G.-H.; García de Arquer, F. P.; Yoon, Y. J.; Lan, X.; Liu, M.; Voznyy, O.; Yang, Z.; Fan, F.; Ip, A. H.; Kanjanaboos, P.; et al. High-Efficiency Colloidal Quantum Dot Photovoltaics via Robust Self-Assembled Monolayers. *Nano Lett.* **2015,** *15*, 7691-7696.

(22) Yuan, M.; Voznyy, O.; Zhitomirsky, D.; Kanjanaboos, P.; Sargent, E. H. Synergistic Doping of Fullerene Electron Transport Layer and Colloidal Quantum Dot Solids Enhances Solar Cell Performance. *Adv. Mater.* **2015,** *27*, 917-921.

(23) Azmi, R.; Oh, S.-H.; Jang, S.-Y. High-Efficiency Colloidal Quantum Dot Photovoltaic Devices Using Chemically Modified Heterojunctions. *ACS Energy Lett.* **2016,** *1*, 100-106.

(24) Hu, L.; Li, D.-B.; Gao, L.; Tan, H.; Chen, C.; Li, K.; Li, M.; Han, J.-B.; Song, H.; Liu, H.; et al. Graphene Doping Improved Device Performance of ZnMgO/PbS Colloidal Quantum Dot Photovoltaics. *Adv. Funct. Mater.* **2016,** *26*, 1899-1907.

(25) Chang, J.; Kuga, Y.; Mora-Sero, I.; Toyoda, T.; Ogomi, Y.; Hayase, S.; Bisquert, J.; Shen, Q. High Reduction of Interfacial Charge Recombination in Colloidal Quantum Dot Solar Cells by Metal Oxide Surface Passivation. *Nanoscale* **2015,** *7*, 5446-5456.

(26) Kemp, K. W.; Labelle, A. J.; Thon, S. M.; Ip, A. H.; Kramer, I. J.; Hoogland, S.; Sargent, E. H. Interface Recombination in Depleted Heterojunction Photovoltaics Based on Colloidal Quantum Dots. *Adv. Energy Mater.* **2013,** *3*, 917-922.

(27) Brown, P. R.; Lunt, R. R.; Zhao, N.; Osedach, T. P.; Wanger, D. D.; Chang, L.-Y.; Bawendi, M. G.; Bulović, V. Improved Current Extraction from ZnO/PbS Quantum Dot Heterojunction Photovoltaics Using a MoO_3 Interfacial Layer. *Nano Lett.* **2011,** *11*, 2955-2961.

(28) Chuang, C.-H. M.; Brown, P. R.; Bulović, V.; Bawendi, M. G. Improved Performance and Stability in Quantum Dot Solar Cells through Band Alignment Engineering. *Nat. Mater.* **2014,** *13*, 796-801.

(29) Ko, D.-K.; Brown, P. R.; Bawendi, M. G.; Bulović, V. p-i-n Heterojunction Solar Cells with a Colloidal Quantum-Dot Absorber Layer. *Adv. Mater.* **2014,** *26*, 4845-4850.

(30) Jin, Z.; Yuan, M.; Li, H.; Yang, H.; Zhou, Q.; Liu, H.; Lan, X.; Liu, M.; Wang, J.; Sargent, E. H.; et al. Graphdiyne: An Efficient Hole Transporter for Stable High-Performance Colloidal Quantum Dot Solar Cells. *Adv. Funct. Mater.* **2016,** *26*, 5284-5289.

(31) Neo, D. C. J.; Zhang, N.; Tazawa, Y.; Jiang, H.; Hughes, G. M.; Grovenor, C. R. M.; Assender, H. E.; Watt, A. A. R. Poly(3-hexylthiophene-2,5-diyl) as a Hole Transport Layer for Colloidal Quantum Dot Solar Cells. *ACS Appl. Mater. Interfaces* **2016,** *8*, 12101-12108.

(32) Zhang, X.; Justo, Y.; Maes, J.; Walravens, W.; Zhang, J.; Liu, J.; Hens, Z.; Johansson, E. M. J. Slow Recombination in Quantum Dot Solid Solar Cell Using p-i-n Architecture with Organic p-Type Hole Transport Material. *J. Mater. Chem. A* **2015,** *3*, 20579-20585.

(33) Irfan; Ding, H.; Gao, Y.; Small, C.; Kim, D. Y.; Subbiah, J.; So, F. Energy Level Evolution of Air and Oxygen Exposed Molybdenum Trioxide Films. *Appl. Phys. Lett.* **2010,** *96*, 243307.

(34) Luther, J. M.; Law, M.; Song, Q.; Perkins, C. L.; Beard, M. C.; Nozik, A. J. Structural, Optical, and Electrical Properties of Self-Assembled Films of PbSe Nanocrystals Treated with 1,2-Ethanedithiol. *ACS Nano* **2008,** *2*, 271-280.

(35) Miller, E. M.; Kroupa, D. M.; Zhang, J.; Schulz, P.; Marshall, A. R.; Kahn, A.; Lany, S.; Luther, J. M.; Beard, M. C.; Perkins, C. L.; et al. Revisiting the Valence and Conduction Band Size Dependence of PbS Quantum Dot Thin Films. *ACS Nano* **2016,** *10*, 3302-3311.

(36) Kim, S.; Im, S. H.; Kang, M.; Heo, J. H.; Seok, S. I.; Kim, S.-W.; Mora-Sero, I.; Bisquert, J. Air-Stable and Efficient Inorganic-Organic Heterojunction Solar Cells Using PbS Colloidal Quantum Dots Co-Capped by 1-Dodecanethiol and Oleic Acid. *Phys. Chem. Chem. Phys.* **2012,** *14*, 14999-15002.

(37) Jumabekov, A. N.; Siegler, T. D.; Cordes, N.; Medina, D. D.; Böhm, D.; Garbus, P.; Meroni, S.; Peter, L. M.; Bein, T. Comparison of Solid-State Quantum-Dot-Sensitized Solar Cells with ex Situ and in Situ Grown PbS Quantum Dots. *J. Phys. Chem. C* **2014,** *118*, 25853-25862.

(38) Lee, H.; Leventis, H. C.; Moon, S.-J.; Chen, P.; Ito, S.; Haque, S. A.; Torres, T.; Nüesch, F.; Geiger, T.; Zakeeruddin, S. M.; et al. PbS and CdS Quantum Dot-Sensitized Solid-State Solar Cells: "Old Concepts, New Results". *Adv. Funct. Mater.* **2009,** *19*, 2735-2742.

(39) Cardona, C. M.; Li, W.; Kaifer, A. E.; Stockdale, D.; Bazan, G. C. Electrochemical Considerations for Determining Absolute Frontier Orbital Energy Levels of Conjugated Polymers for Solar Cell Applications. *Adv. Mater.* **2011,** *23*, 2367-2371.

(40) Wu, G.; Kaneko, R.; Islam, A.; Zhang, Y.; Sugawa, K.; Han, L.; Shen, Q.; Bedja, I.; Gupta, R. K.; Otsuki, J. Thiocyanate-Free Asymmetric Ruthenium(II) Dye Sensitizers Containing Azole Chromophores with Near-IR Light-Harvesting Capacity. *J. Power Sources* **2016,** *331*, 100-111.

(41) Wu, G.; Kaneko, R.; Zhang, Y.; Shinozaki, Y.; Sugawa, K.; Islam, A.; Han, L.; Bedja, I.; Gupta, R. K.; Shen, Q.; et al. Neutral and Anionic Tetrazole-Based Ligands in Designing Novel Ruthenium Dyes for Dye-Sensitized Solar Cells. *J. Power Sources* **2016,** *307*, 416-425.

(42) Brauer, J. C.; Lee, Y. H.; Nazeeruddin, M. K.; Banerji, N. Charge Transfer Dynamics from Organometal Halide Perovskite to Polymeric Hole Transport Materials in Hybrid Solar Cells. *J. Phys. Chem. Lett.* **2015,** *6*, 3675-3681.

(43) Zhang, F.; Zhao, X.; Yi, C.; Bi, D.; Bi, X.; Wei, P.; Liu, X.; Wang, S.; Li, X.; Zakeeruddin, S. M.; et al. Dopant-Free Star-Shaped Hole-Transport Materials for Efficient and Stable Perovskite Solar Cells. *Dyes Pigm.* **2017,** *136*, 273-277.

(44) Jasieniak, J.; Califano, M.; Watkins, S. E. Size-Dependent Valence and Conduction Band-Edge Energies of Semiconductor Nanocrystals. *ACS Nano* **2011,** *5*, 5888-5902.

(45) Zhang, Y.; Ding, C.; Wu, G.; Nakazawa, N.; Chang, J.; Ogomi, Y.; Toyoda, T.; Hayase, S.; Katayama, K.; Shen, Q. Air Stable PbSe Colloidal Quantum Dot Heterojunction Solar Cells: Ligand-Dependent Exciton Dissociation, Recombination, Photovoltaic Property, and Stability. *J. Phys. Chem. C* **2016,** *120*, 28509-28518.

(46) Zaban, A.; Greenshtein, M.; Bisquert, J. Determination of the Electron Lifetime in Nanocrystalline Dye Solar Cells by Open-Circuit Voltage Decay Measurements. *ChemPhysChem* **2003,** *4*, 859-864.

(47) Bisquert, J.; Fabregat-Santiago, F.; Mora-Seró, I.; Garcia-Belmonte, G.; Giménez, S. Electron Lifetime in Dye-Sensitized Solar Cells: Theory and Interpretation of Measurements. *J. Phys. Chem. C* **2009,** *113*, 17278-17290.

(48) Wang, H.; Gonzalez-Pedro, V.; Kubo, T.; Fabregat-Santiago, F.; Bisquert, J.; Sanehira, Y.; Nakazaki, J.; Segawa, H. Enhanced Carrier Transport Distance in Colloidal PbS Quantum-Dot-Based Solar Cells Using ZnO Nanowires. *J. Phys. Chem. C* **2015,** *119*, 27265-27274.

(49) Connelly, N. G.; Geiger, W. E. Chemical Redox Agents for Organometallic Chemistry. *Chem. Rev.* **1996,** *96*, 877-910.